



# *N,N'*-Bis(pyridin-4-ylmethyl)oxalamide benzene monosolvate: crystal structure, Hirshfeld surface analysis and computational study

Sang Loon Tan, Nathan R. Halcovitch and Edward R. T. Tiekink

*Acta Cryst.* (2019). E75, 1133–1139



IUCr Journals

CRYSTALLOGRAPHY JOURNALS ONLINE

This open-access article is distributed under the terms of the Creative Commons Attribution Licence <http://creativecommons.org/licenses/by/4.0/legalcode>, which permits unrestricted use, distribution, and reproduction in any medium, provided the original authors and source are cited.





# *N,N'*-Bis(pyridin-4-ylmethyl)oxalamide benzene monosolvate: crystal structure, Hirshfeld surface analysis and computational study

Sang Loon Tan,<sup>a‡</sup> Nathan R. Halcovitch<sup>b</sup> and Edward R. T. Tiekink<sup>a\*</sup>

<sup>a</sup>Research Centre for Crystalline Materials, School of Science and Technology, Sunway University, 47500 Bandar Sunway, Selangor Darul Ehsan, Malaysia, and <sup>b</sup>Department of Chemistry, Lancaster University, Lancaster LA1 4YB, United Kingdom. \*Correspondence e-mail: edwardt@sunway.edu.my

Received 25 June 2019

Accepted 3 July 2019

Edited by W. T. A. Harrison, University of Aberdeen, Scotland

‡ Additional correspondence author, e-mail: alant@sunway.edu.my.

**Keywords:** crystal structure; bis(4-pyridylmethyl)oxalamide; benzene solvate; hydrogen bonding; Hirshfeld surface analysis; computational chemistry.

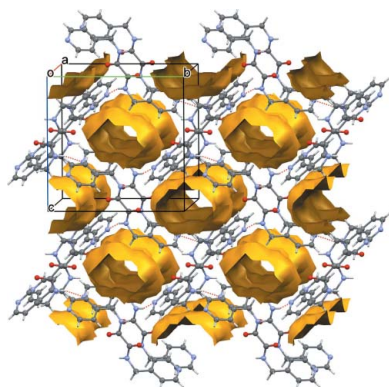
**CCDC reference:** 1938031

**Supporting information:** this article has supporting information at journals.iucr.org/e

The asymmetric unit of the title 1:1 solvate,  $C_{14}H_{14}N_4O_2 \cdot C_6H_6$  [systematic name of the oxalamide molecule: *N,N'*-bis(pyridin-4-ylmethyl)ethanediamide], comprises a half molecule of each constituent as each is disposed about a centre of inversion. In the oxalamide molecule, the central  $C_2N_2O_2$  atoms are planar (r.m.s. deviation = 0.0006 Å). An intramolecular amide-N—H $\cdots$ O(amide) hydrogen bond is evident, which gives rise to an *S*(5) loop. Overall, the molecule adopts an antiperiplanar disposition of the pyridyl rings, and an orthogonal relationship is evident between the central plane and each terminal pyridyl ring [dihedral angle = 86.89 (3)°]. In the crystal, supramolecular layers parallel to (10 $\bar{2}$ ) are generated owing the formation of amide-N—H $\cdots$ N(pyridyl) hydrogen bonds. The layers stack encompassing benzene molecules which provide the links between layers *via* methylene-C—H $\cdots$  $\pi$ (benzene) and benzene-C—H $\cdots$  $\pi$ (pyridyl) interactions. The specified contacts are indicated in an analysis of the calculated Hirshfeld surfaces. The energy of stabilization provided by the conventional hydrogen bonding (approximately 40 kJ mol<sup>-1</sup>; electrostatic forces) is just over double that by the C—H $\cdots$  $\pi$  contacts (dispersion forces).

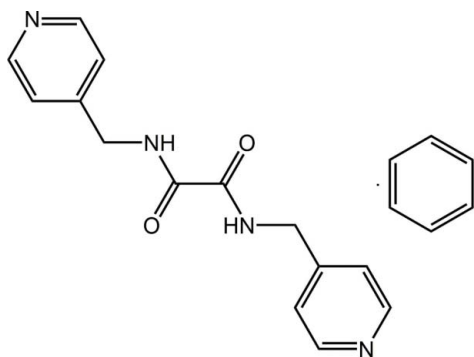
## 1. Chemical context

With a combination of centrally located amide and terminal pyridyl functional groups, the isomeric molecules related to the title compound of the general formula (*n*-C<sub>5</sub>H<sub>4</sub>N)CH<sub>2</sub>N(H)C(=O)C(=O)N(H)CH<sub>2</sub>(C<sub>5</sub>H<sub>4</sub>N-*n*), for *n* = 2, 3 and 4, abbreviated as <sup>*n*</sup>LH<sub>2</sub>, have long attracted the attention of structural chemists and their structural chemistry has been reviewed very recently (Tiekink, 2017). Taking the <sup>3</sup>LH<sub>2</sub> species as an exemplar, its 1:1 co-crystal with *N,N'*-dicarboxymethylurea, HO<sub>2</sub>CCH<sub>2</sub>N(H)C(=O)N(H)CH<sub>2</sub>CO<sub>2</sub>H, features two distinct supramolecular tapes sustained by N—H $\cdots$ O hydrogen bonding. The first of these arises from amide-N—H $\cdots$ O(amide) hydrogen bonding between the amide groups, on both sides of the <sup>3</sup>LH<sub>2</sub> molecule, through ten-membered amide synthons { $\cdots$ HNC<sub>2</sub>O<sub>2</sub>}<sub>2</sub> (Nguyen *et al.*, 2001). Parallel tapes comprising *N,N'*-dicarboxymethylurea molecules, sustained by six-membered { $\cdots$ O $\cdots$ HNCNH} synthons, are also formed. The links between the tapes leading to a two-dimensional array are of the type hydroxy-O—H $\cdots$ N(pyridyl). Molecules of <sup>*n*</sup>LH<sub>2</sub> also featured prominently in early, systematic studies of halogen bonding. An illustrative example is found in the 1:1 co-crystal formed between <sup>3</sup>LH<sub>2</sub> and 1,4-di-iodobuta-1,3-diyne, I—C $\equiv$ C—C $\equiv$ C—I (Goroff *et al.*, 2005). A two-dimensional array is also found in



OPEN ACCESS

this co-crystal whereby supramolecular tapes between  ${}^3\text{LH}_2$  molecules are formed as for the previous example and these are connected by  $\text{N}\cdots\text{I}$  halogen bonding. In the crystals of both polymorphs of pure  ${}^3\text{LH}_2$  (Jotani *et al.*, 2016), similar supramolecular tapes mediated by amide hydrogen bonding are formed. However, that this mode of supramolecular association is not all pervasive in the  ${}^n\text{LH}_2$  systems is seen the structures of the two polymorphs of pure  ${}^4\text{LH}_2$  (Lee & Wang, 2007; Lee, 2010). In one of the polymorphs of this isomer, supramolecular dimers are formed *via* amide-N—H $\cdots$ O(amide) hydrogen bonding and these are linked into a two-dimensional array *via* amide-N—H $\cdots$ N(pyridyl) hydrogen bonds (Lee & Wang, 2007). In the second polymorph, all potential amide-N—H and pyridyl-N donors and acceptors associate *via* amide-N—H $\cdots$ N(pyridyl) hydrogen bonds to generate a two-dimensional array. In this context, and in the context of recent work on  ${}^4\text{LH}_2$  in co-crystals (Syed *et al.*, 2016) and adducts of zinc 1,1-dithiolates (Arman *et al.*, 2018; Tan, Chun *et al.*, 2019), it was thought of interest to conduct a polymorph screen for  ${}^4\text{LH}_2$ . From a series of crystallizations of  ${}^4\text{LH}_2$  taken in dimethylformamide and layered with benzene, *o*-xylene, *m*-xylene, *p*-xylene, toluene, pyridine and cyclohexane in separate experiments, only crystals of the title benzene solvate, (I), were isolated. Herein, the crystal and molecular structures of (I) are described along with a further evaluation of the supramolecular association *via* an analysis of the calculated Hirshfeld surfaces as well as a computational chemistry study.



## 2. Structural commentary

The title co-crystal (I) is the result of crystallization of  ${}^4\text{LH}_2$ , taken in dimethylformamide, with benzene. The crystallographic asymmetric unit comprises half a molecule each of  ${}^4\text{LH}_2$  and benzene, Fig. 1, each being disposed about a crystallographic centre of inversion. The central  $\text{C}_2\text{N}_2\text{O}_2$  plane is strictly planar with the r.m.s. deviation of the fitted atoms being 0.0006 Å; the C7 atoms lie 0.0020 (16) Å to either side of the plane. An intramolecular amide-N—H $\cdots$ O(amide)<sup>i</sup> hydrogen bond, occurring between the symmetry related amide groups, gives rise to an *S*(5) loop, Table 1; symmetry operation (i)  $1 - x$ ,  $1 - y$ ,  $-z$ . The crystallographic symmetry also implies an antiperiplanar disposition of the pyridyl rings. The dihedral angle between the central plane and terminal pyridyl ring is 86.89 (3)°, indicating an orthogonal relationship.

**Table 1**  
Hydrogen-bond geometry (Å, °).

Cg1 is the centroid of the centrosymmetric (C11–C13, C11<sup>i</sup>–C13<sup>i</sup>) ring. Cg2 is the ring centroid of the (N1, C2–C5) ring.

$D\text{—}H\cdots A$	$D\text{—}H$	$H\cdots A$	$D\cdots A$	$D\text{—}H\cdots A$
N8—H8N $\cdots$ O10 <sup>i</sup>	0.89 (1)	2.36 (1)	2.7129 (11)	104 (1)
N8—H8N $\cdots$ N1 <sup>ii</sup>	0.89 (1)	2.03 (1)	2.8737 (12)	159 (1)
C7—H7B $\cdots$ Cg1	0.99	2.62	3.4037 (11)	136
C11—H11 $\cdots$ Cg2 <sup>iii</sup>	0.95	2.90	3.6361 (11)	136

Symmetry codes: (i)  $-x + 1, -y + 1, -z$ ; (ii)  $-x + 2, y + \frac{1}{2}, -z + \frac{1}{2}$ ; (iii)  $-x + 1, y + \frac{1}{2}, -z + \frac{1}{2}$ .

## 3. Supramolecular features

The geometric parameters characterizing the interatomic contacts identified in the crystal of (I) are given in Table 1. The key feature of the molecular packing is the formation of amide-N—H $\cdots$ N(pyridyl) hydrogen bonding. This generates a two-dimensional, rectangular grid lying parallel to  $(10\bar{2})$ , Fig. 2(a), with dimensions defined by O10 $\cdots$ O10 and N8 $\cdots$ N8 separations of 9.6770 (11) and 12.3255 (11) Å, respectively. The other notable contacts in the crystal are of the type C—H $\cdots$  $\pi$ , Table 1. Thus, methylene-C7—H $\cdots$  $\pi$ (benzene) and benzene-C11—H $\cdots$  $\pi$ (pyridyl) interactions are formed. From symmetry, each benzene molecule forms four, *i.e.* two (as acceptor) and two (as donor), such interactions, Fig. 2(b). The side-on view of Fig. 2(b) shown in Fig. 2(c) indicates the amide-N—H and pyridyl-N project in all directions around the five-molecule aggregate. Indeed, it is the C—H $\cdots$  $\pi$  interactions that connect the layers into a three-dimensional architecture, Fig. 2(d).

Upon removing the benzene molecules within a  $2 \times 2 \times 2$  set of unit cells, the packing was subjected to a calculation of solvent-accessible void space in *Mercury* (Macrae *et al.*, 2006) with a probing radius of 1.2 Å. The results showed that the packing devoid of benzene comprises approximately 25.8% of

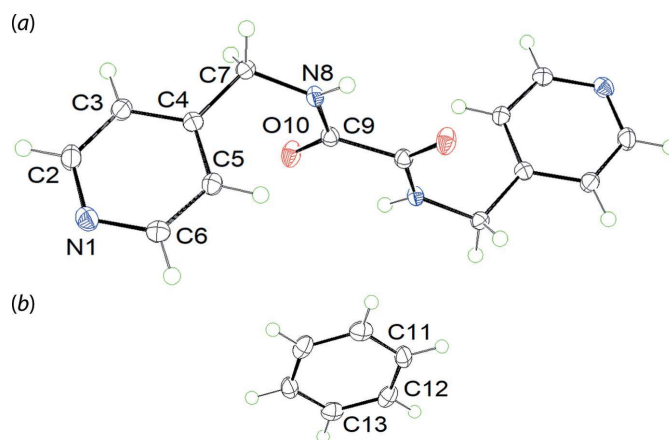


**Figure 1**  
The molecular structures of the constituents of the asymmetric unit of (I), showing the atom-labelling scheme and displacement ellipsoids at the 50% probability level. The molecules are each disposed about a centre of inversion with the unlabelled atoms in (a) related by the symmetry operation:  $1 - x$ ,  $1 - y$ ,  $-z$  and those in (b) related by  $1 - x$ ,  $1 - y$ ,  $1 - z$ .

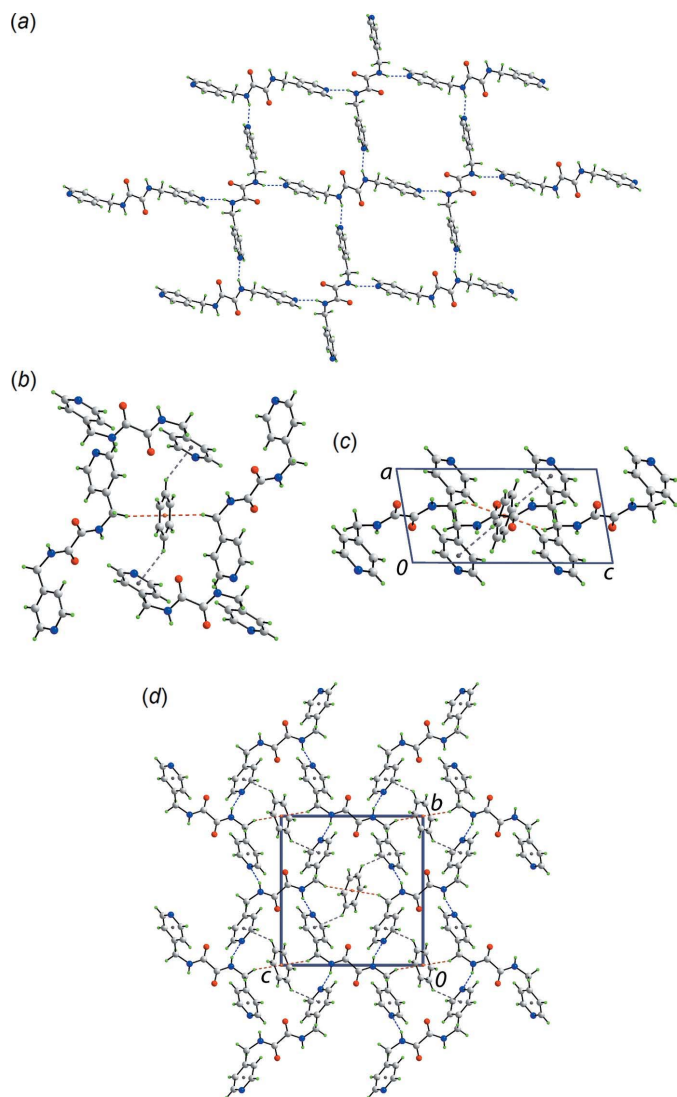


**Figure 2**  
Molecular packing in (I): (a) a view of the square grid sustained by amide-N—H···N(pyridyl) hydrogen bonding shown as blue dashed lines, (b) a view of the five-molecule aggregate connected by methylene-C—H···π(benzene) and benzene-C—H···π(pyridyl) interactions, shown as orange and purple dashed lines, respectively, (c) side-on view of the five-molecule aggregate and (d) a view of the unit-cell contents shown in projection down the *a* axis.

the volume which is equivalent to  $227.3 \text{ \AA}^3$  of void space, as illustrated in Fig. 3.

#### 4. Hirshfeld surface analysis and computational study

To gain a better understanding of the nature of the intermolecular interactions identified in (I), the overall structure of (I) as well as the individual  $^4\text{LH}_2$  and benzene molecules were subjected to a Hirshfeld surface analysis using *Crystal Explorer 17* (Turner *et al.*, 2017) based on the procedures as described in the literature (Tan, Jotani *et al.*, 2019).

The Hirshfeld surface mapped over  $d_{\text{norm}}$  map of  $^4\text{LH}_2$  displays several red spots, that range from intense to weak,

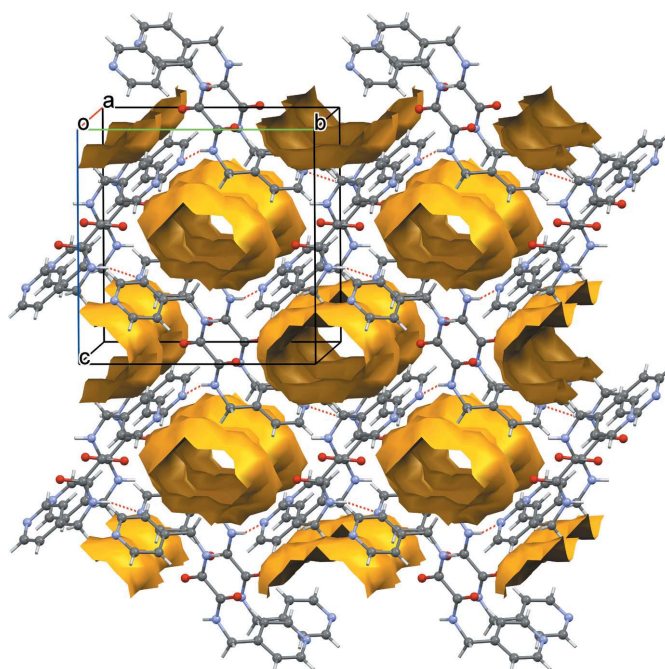


**Figure 3**  
A plot of the solvent-accessible voids in the crystal of (I) upon removal of the solvent benzene molecules within a  $2 \times 2 \times 2$  set of unit cells.

which reflect the interactions identified in the crystal (Spackman & Jayatilaka, 2009). The intense red spots arise from amide-N—H···N(pyridyl) hydrogen bonds while the diminutive spots originate from methylene-C7—H7B···π(benzene) interactions, Fig. 4(a), with both indicative of contact distances shorter than the respective sum of the van der Waals radii. Reflecting the relatively long separation, the benzene-C11—H11···π(pyridyl) interaction is reflected as

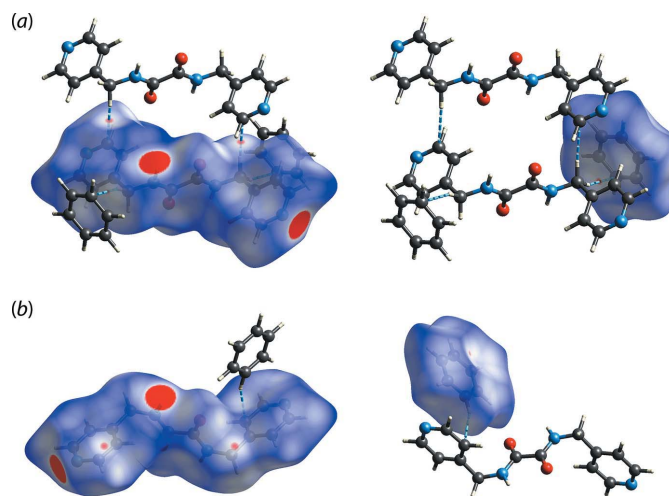


**Figure 4**  
The  $d_{\text{norm}}$  maps within the range of  $-0.0567$  to  $0.9466$  arbitrary units for the  $^4\text{LH}_2$  (left) and benzene (right) molecules: (a) highlighting the amide-N—H···N(pyridyl) (intense red) and methylene-C7—H7B···π(benzene) (faint red) contacts with the intensity relative to the contact distance and (b) highlighting the connections between molecules mediated by benzene-C11—H11···π(pyridyl) interactions.

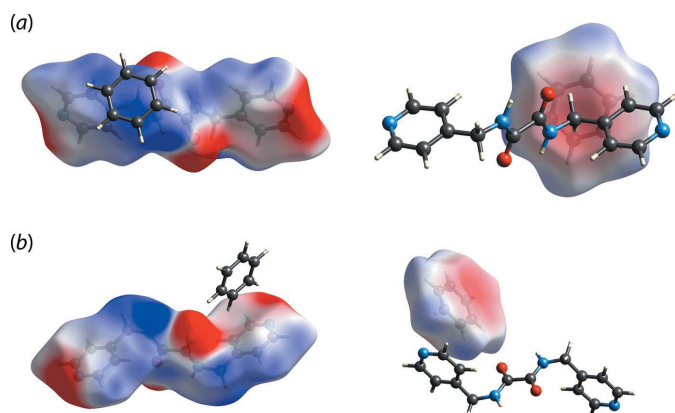


**Figure 5**  
The calculated electrostatic potential mapped onto the Hirshfeld surfaces with the isosurface value range of  $-0.0257$  to  $0.0389$  atomic unit for the  ${}^4\text{LH}_2$  (left) and benzene (right) molecules showing the charge complementarity for the (a) methylene-C7–H7B $\cdots\pi$ (benzene) and (b) benzene-C11–H11 $\cdots\pi$ (pyridyl) interactions.

only a white spot as the contact distance is only just within the sum of van der Waals radii, as shown in Fig. 4(b).

The C–H $\cdots\pi$  interactions were subjected to electrostatic potential mapping for verification purposes. The result shows that the methylene-C7–H7B $\cdots\pi$ (benzene) contact is indeed electrostatic in nature as revealed by the distinct blue (*i.e.* electropositive) and red (*i.e.* electronegative) colour scheme on the surface of the contact points, Fig. 5(a). In contrast, the benzene-C11–H11 $\cdots\pi$ (pyridyl) contact displays pale colouration around the contact zone suggesting that the interaction could be attributed to weak dispersion forces, Fig. 5(b).

The two-dimensional fingerprint plots were generated for overall (I) as well as its individual molecules to quantify the close contacts identified through the Hirshfeld surface analysis, see Fig. 6(a)–(e). As shown in the overall fingerprint plot in Fig. 6(a), (I) exhibits a bug-like profile with distinctive symmetrical spikes which are similar to those exhibited by the individual  ${}^4\text{LH}_2$  molecule, therefore indicating that the intermolecular interactions in (I) are mainly sustained by  ${}^4\text{LH}_2$  molecules. Decomposition of the overall fingerprint plots of (I) shows that the contacts are mainly dominated by H $\cdots$ H (45.1%;  $d_i + d_e \sim 2.42$  Å), H $\cdots$ C/C $\cdots$ H (26.6%;  $d_i + d_e \sim 2.66$  Å), H $\cdots$ O/O $\cdots$ H (14.4%;  $d_i + d_e \sim 2.58$  Å), H $\cdots$ N/N $\cdots$ H (13.1%;  $d_i + d_e \sim 1.88$  Å) and other contacts (0.8%). Except for the H $\cdots$ H contacts, to differing extents, the remaining major contacts are shorter than the corresponding sum of van der Waals radii for H $\cdots$ C ( $\sim 2.90$  Å), H $\cdots$ O ( $\sim 2.72$  Å) and H $\cdots$ N ( $\sim 2.75$  Å).

The individual  ${}^4\text{LH}_2$  molecule exhibits at similar distribution of the major contacts compared to overall (I). However, some distinctions are observed on the external and internal contacts upon further delineation of the corresponding decomposed fingerprint plots. While the distribution is rather symmetric in overall (I), for  ${}^4\text{LH}_2$  these are either inclined towards the external or internal contacts presumably due to interaction with the solvent benzene molecule. For instance,

the H $\cdots$ C/C $\cdots$ H contact in the individual  ${}^4\text{LH}_2$  molecule comprises 9.9% (internal)-H $\cdots$ C-(external) and 14.6% (internal)-C $\cdots$ H-(external) contacts as compared to 12.0 and 14.6% for the equivalent contacts in overall (I), Fig. 6(c). Similar observations pertain for the H $\cdots$ O/O $\cdots$ H and H $\cdots$ N/N $\cdots$ H interactions, Fig. 6(d)–(e).

As for the benzene molecule, an irregular fingerprint profile is noted with the distribution dominated by H $\cdots$ H (46.4%) and H $\cdots$ C/C $\cdots$ H (41.9%) surface contacts. The latter are almost equally distributed between the internal and external contacts, *i.e.* 20.5% for (internal)-H $\cdots$ C-(external) and 21.4% for (internal)-C $\cdots$ H-(external) contacts. In addition, the solvent molecules are sustained in the molecular architecture through minor contributions from H $\cdots$ O (5.6%) and H $\cdots$ N (5.9%) contacts, respectively. These interactions are at distances of  $\sim 2.52$  Å (H $\cdots$ H),  $\sim 2.92$  Å (H $\cdots$ C/C $\cdots$ H),  $\sim 2.98$  Å (H $\cdots$ O) and  $\sim 2.79$  Å (H $\cdots$ N), which are greater than the corresponding sum of van der Waals radii, indicating

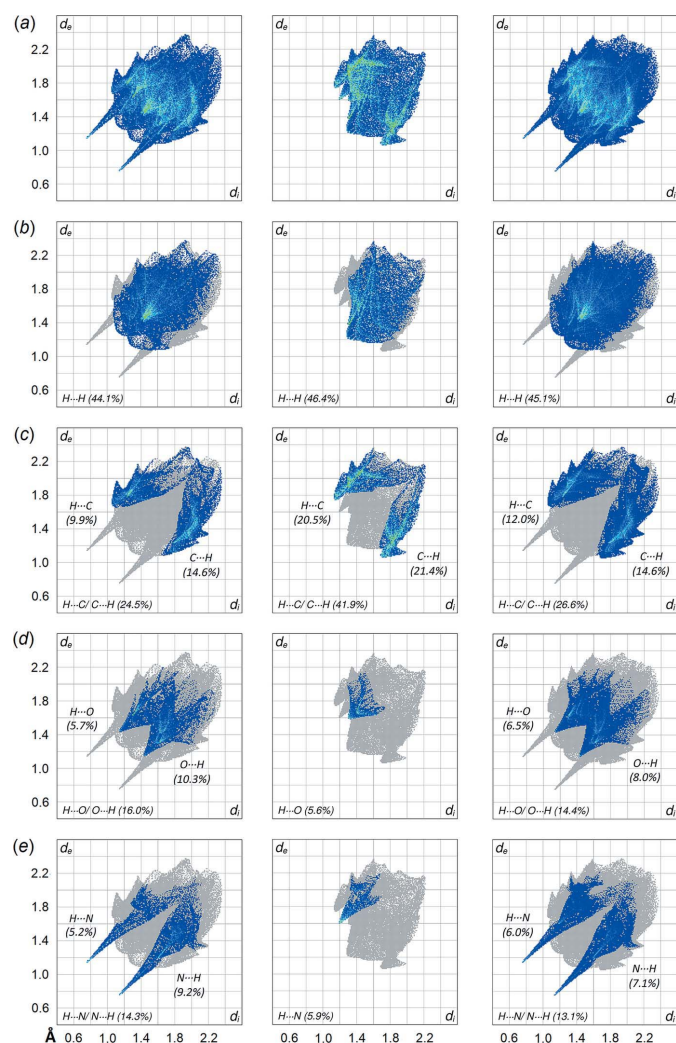


**Figure 6**  
(a) The overall two-dimensional fingerprint plots for  ${}^4\text{LH}_2$ , benzene and overall (I), and those delineated into (b) H $\cdots$ H, (c) H $\cdots$ C/C $\cdots$ H, (d) H $\cdots$ O/O $\cdots$ H and (e) H $\cdots$ N/N $\cdots$ H, with the percentage contribution being specified for each contact indicated therein.

**Table 2**  
Interaction energies (kJ mol<sup>-1</sup>) for selected close contacts.

Close contact	$E_{\text{electrostatic}}$	$E_{\text{polarization}}$	$E_{\text{dispersion}}$	$E_{\text{exchange-repulsion}}$	$E_{\text{total}}$	Symmetry operation
N8—H8···N1	-45.0	-12.2	-17.5	54.7	-38.1	$-x + 2, y + \frac{1}{2}, -z + \frac{1}{2}$
C7—H7B···Cg(benzene)	-10.1	-2.1	-23.7	22.6	-18.9	$x, y, z$
C11—H11···Cg(pyridyl)	-5.2	-1.1	-15.3	4.4	-16.9	$-x + 1, y + \frac{1}{2}, -z + \frac{1}{2}$

**Table 3**  
Selected geometric data (Å, °) for molecules of <sup>4</sup>LH<sub>2</sub>.

Crystal	Z	central-C—C—central	C <sub>2</sub> N <sub>2</sub> O <sub>2</sub> /C <sub>5</sub> H <sub>4</sub> N	C <sub>2</sub> N <sub>2</sub> O <sub>2</sub> /C <sub>5</sub> H <sub>4</sub> N	Reference
Form I – molecule <i>a</i>	2	1.541 (3)	84.59 (6) & 80.33 (4)	4.90 (6)	Lee & Wang (2007)
Form I – molecule <i>b</i>		1.541 (3)	70.20 (5) & 68.01 (5)	6.68 (6)	
Form II	0.5	1.532 (2)	74.78 (4)	0	Lee (2010)
Benzene solvate (I)	0.5	1.5406 (18)	86.89 (3)	0	This work

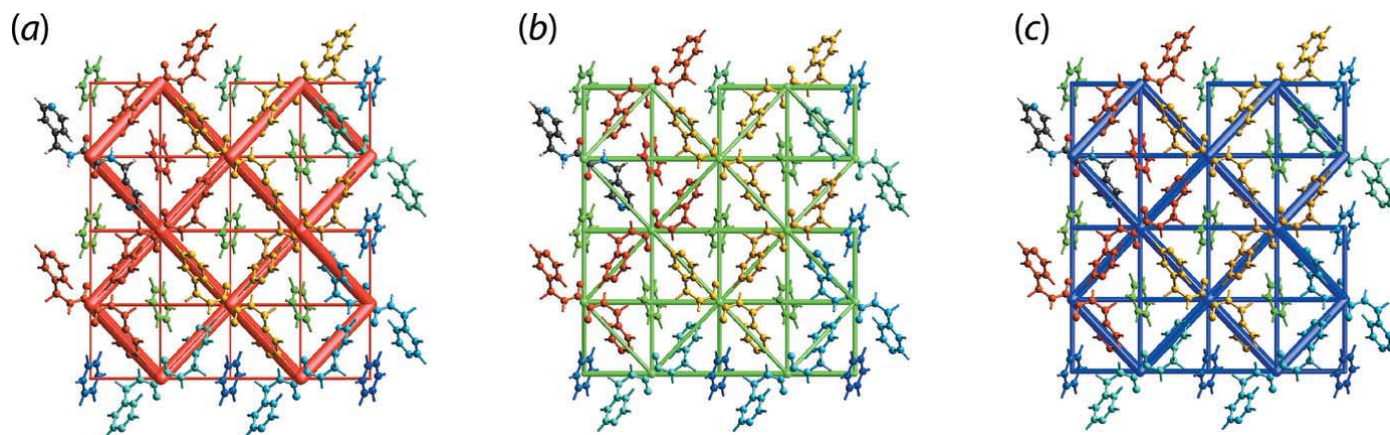
the identified C—H···π(benzene and pyridyl) interactions can largely be considered as localized interactions.

## 5. Computational chemistry study

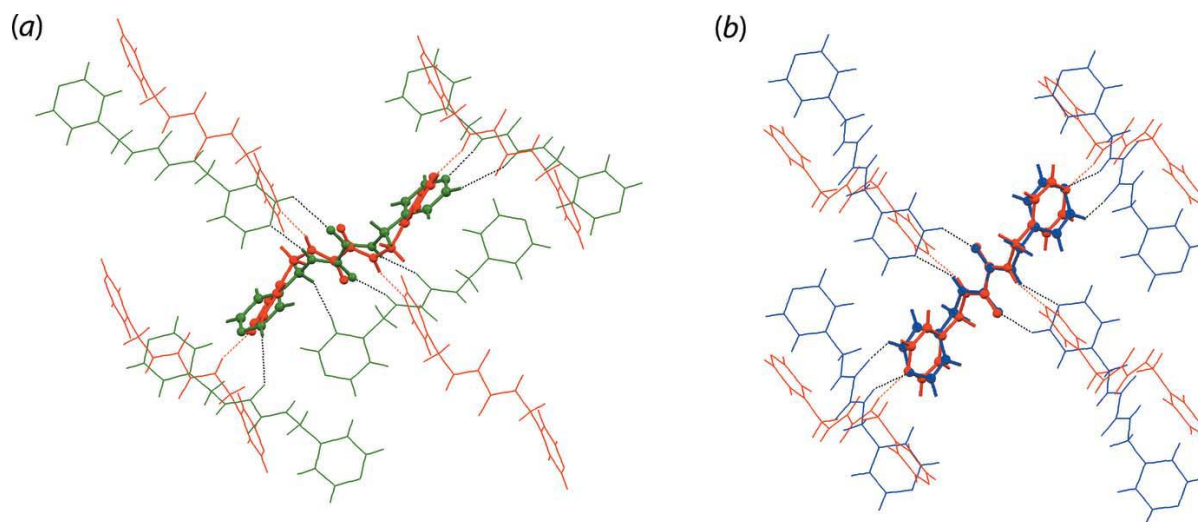
The calculation of interaction energy was performed using *Crystal Explorer 17* based on the procedures as described previously (Tan, Jotani *et al.*, 2019). As expected, the greatest interaction energy in the crystal of (I) is found for the amide-N—H···N(pyridyl) contact having a total energy ( $E_{\text{int}}$ ) of -38.1 kJ mol<sup>-1</sup>, Table 2. This is followed by methylene-C7—H7B···π(benzene) and benzene-C11—H11···π(pyridyl) contacts with a very similar  $E_{\text{int}}$  values of -18.9 and -16.9 kJ mol<sup>-1</sup>, respectively, despite the  $d_{\text{norm}}$  contact distance being significantly greater for the latter. The calculation results reveal that the repulsion energy is greater in methylene-C7—H7B···π(benzene) compared with the benzene-C11—H11···π(pyridyl) contact, which contributes to the slight variation in their  $E_{\text{int}}$  values. In short, the N—H···N interaction is stabilized largely by electrostatic forces while the C—H···π interactions are stabilized largely by dispersion

forces. Overall, the crystal of (I) is dominated by electrostatic forces that form a cross-shaped energy framework that encompasses the void space in the unit cell. This framework is further stabilized by dispersion forces that co-exist within the void owing to the weaker interactions between the solvent molecules with the host, Fig. 7(a)–(c).

Calculations were also performed to compare the molecular packing similarity of (I) with the two polymorphic forms of <sup>4</sup>LH<sub>2</sub> available in the literature (Lee & Wang, 2007; Lee, 2010). Molecular clusters of (I), Form I and Form II containing 20 <sup>4</sup>LH<sub>2</sub> molecules each were subjected to molecular packing analysis using *Mercury* (Macrae *et al.*, 2006), with the geometric tolerances being set to 20% (*i.e.* only molecules within the 20% tolerance for both distances and angles were included in the calculation and molecules with a variation >20% were discarded); molecular inversions were enabled during calculation. The result shows that out of the 20 molecules in the cluster, only one <sup>4</sup>LH<sub>2</sub> molecule in each polymorph resembled the reference packing in (I) with an r.m.s. deviation of 0.587 and 0.403 Å, respectively, Fig. 8(a) and (b). The result clearly demonstrates the influence of solvent molecule upon the molecular packing in (I).



**Figure 7**  
Energy framework of (I) as viewed down along the *a*-axis direction, showing the (a) electrostatic potential force, (b) dispersion force and (c) total energy diagrams. The cylindrical radii are proportional to the relative strength of the corresponding energies and they were adjusted to the same scale factor of 120 with a cut-off value of 5 kJ mol<sup>-1</sup> within 2 × 2 × 2 unit cells.


**Figure 8**

A comparison of molecular packing of  ${}^4\text{LH}_2$ : (a) (I) (red image) and Form I (green) and (b) (I) (red) and Form II (blue), showing the differences between five pairs of  ${}^4\text{LH}_2$  molecules with an overall r.m.s. deviation of 0.587 and 0.403 Å, respectively.

Finally, and referring to Fig. 9, (I) and the two polymorphic forms of  ${}^4\text{LH}_2$  exhibit a close similarity in the distribution of molecular contacts as judged from the percentage contribution of the corresponding contacts on the Hirshfeld surface. The maximum variation in the distribution of  $\text{H}\cdots\text{H}$ ,  $\text{H}\cdots\text{C}/\text{C}\cdots\text{H}$ ,  $\text{H}\cdots\text{O}/\text{O}\cdots\text{H}$  and  $\text{H}\cdots\text{N}/\text{N}\cdots\text{H}$  contacts ranged from 7.1, 4.9, 2.2 and 3.8%, respectively among the three crystals.

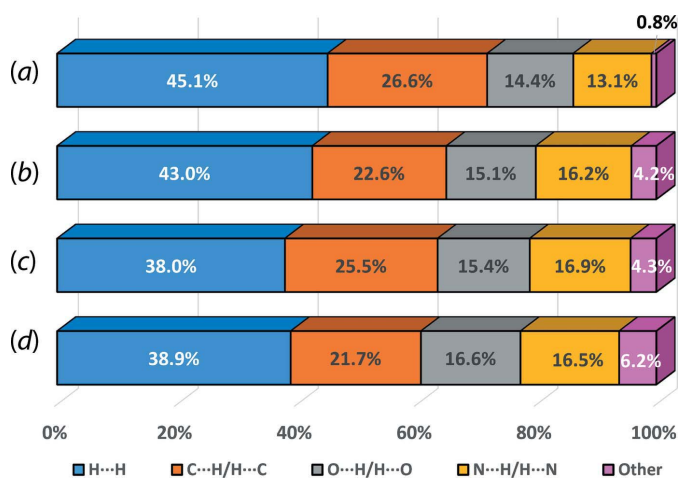
## 6. Database survey

As mentioned in the *Chemical Context*, there are two polymorphs available for  ${}^4\text{LH}_2$  (Lee & Wang, 2007; Lee, 2010). In Form I (Lee & Wang, 2007), two independent molecules comprise the asymmetric unit whereas in Form II (Lee, 2010), half a centrosymmetric molecule comprises the asymmetric unit. Selected geometric parameters for the polymorphs and

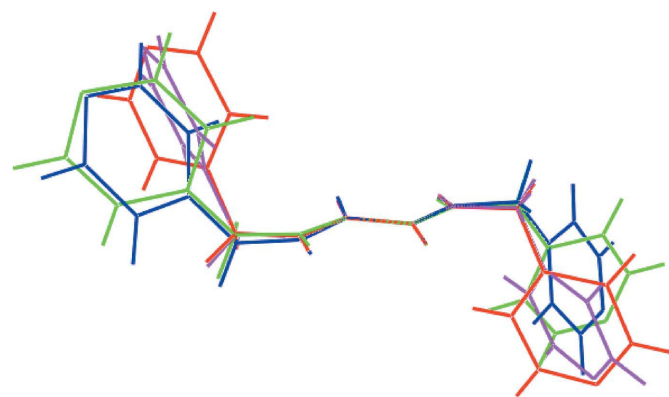
(I) are given in Table 3. To a first approximation, the molecular structures present the same geometric features, *i.e.* a planar central region and an antiperiplanar relationship between the pyridyl rings. It is noted that the central C—C bond is relatively long, a consistent observation traced to the influence of electronegative carbonyl-O and amide-N substituents and confirmed by DFT calculations in the case of polymorphic  ${}^3\text{LH}_2$  (Jotani *et al.*, 2016) and in the sulfur analogues of  ${}^3\text{LH}_2$ , *i.e.* ( $n\text{-C}_5\text{H}_4\text{N}$ ) $\text{CH}_2\text{N}(\text{H})\text{C}(=\text{S})\text{C}(=\text{S})\text{N}(\text{H})\text{CH}_2(\text{C}_5\text{H}_4\text{N}-n)$ , for  $n = 2, 3$  and 4 (Zukerman-Schpector *et al.*, 2015). The similarity between the four molecules of  ${}^4\text{LH}_2$  in its polymorphs and benzene solvate are highlighted in Fig. 10.

## 7. Synthesis and crystallization

The precursor, *N,N'*-bis(pyridin-4-ylmethyl)oxalamide, was prepared in accordance with the literature procedure (m.p. 486.3–487.6 K; lit. 486–487 K; Nguyen *et al.*, 1998): it (0.0015 g)


**Figure 9**

Percentage distribution of the corresponding close contacts on the Hirshfeld surfaces of  ${}^4\text{LH}_2$  in (a) (I), (b) Form I – first independent molecule, (c) Form I – second independent molecule and (d) Form II.


**Figure 10**

Overlay diagram for  ${}^4\text{LH}_2$  molecules in Form I – molecule *a* (green image), Form I – molecule *b* (blue), Form II (pink) and benzene solvate (red).

**Table 4**  
Experimental details.

Crystal data	
Chemical formula	C <sub>14</sub> H <sub>14</sub> N <sub>4</sub> O <sub>2</sub> ·C <sub>6</sub> H <sub>6</sub>
<i>M</i> <sub>r</sub>	348.40
Crystal system, space group	Monoclinic, <i>P</i> 2 <sub>1</sub> / <i>c</i>
Temperature (K)	100
<i>a</i> , <i>b</i> , <i>c</i> (Å)	5.80832 (8), 12.6437 (2), 12.1803 (2)
β (°)	99.942 (1)
<i>V</i> (Å <sup>3</sup> )	881.07 (2)
<i>Z</i>	2
Radiation type	Cu <i>K</i> α
μ (mm <sup>-1</sup> )	0.71
Crystal size (mm)	0.27 × 0.22 × 0.16
Data collection	
Diffraction	Rigaku Oxford Diffraction Super-
Instrument	Nova, Dual, Cu at zero, AtlasS2
Absorption correction	Multi-scan ( <i>CrysAlis PRO</i> ; Rigaku
	OD, 2015)
<i>T</i> <sub>min</sub> , <i>T</i> <sub>max</sub>	0.917, 1.000
No. of measured, independent and observed [ <i>I</i> > 2σ( <i>I</i> )] reflections	7547, 1838, 1741
<i>R</i> <sub>int</sub>	0.018
(sin θ/λ) <sub>max</sub> (Å <sup>-1</sup> )	0.630
Refinement	
<i>R</i> [ <i>F</i> <sup>2</sup> > 2σ( <i>F</i> <sup>2</sup> )], <i>wR</i> ( <i>F</i> <sup>2</sup> ), <i>S</i>	0.034, 0.092, 1.03
No. of reflections	1838
No. of parameters	121
No. of restraints	1
H-atom treatment	H atoms treated by a mixture of independent and constrained refinement
Δρ <sub>max</sub> , Δρ <sub>min</sub> (e Å <sup>-3</sup> )	0.26, -0.22

Computer programs: *CrysAlis PRO* (Rigaku OD, 2015), *SHELXT* (Sheldrick, 2015a), *SHELXL2018* (Sheldrick, 2015b), *ORTEP-3 for Windows* (Farrugia, 2012), *OLEX2* (Dolomanov *et al.*, 2009), *Mercury* (Macrae *et al.*, 2006), *DIAMOND* (Brandenburg, 2006) and *QMol* (Gans & Shalloway, 2001) and *pubCIF* (Westrip, 2010).

was dissolved in DMF (0.5 ml) and then carefully layered in different experiments with 2 ml of benzene, *o*-xylene, *m*-xylene, *p*-xylene, toluene, pyridine and cyclohexane. Among these solvent systems, only the DMF–benzene mixture resulted in colourless crystals of the benzene solvate, (I); m.p. 411.4–413.7 K. IR (cm<sup>-1</sup>): 3322 ν(N–H), 3141–2804 ν(C–H), 1696–1661 ν(C=O), 1563–1515 ν(C=C), 1414 ν(C–N), 794 δ(C=C).

## 8. Refinement

Crystal data, data collection and structure refinement details are summarized in Table 4. The carbon-bound H atoms were placed in calculated positions (C–H = 0.95–0.99 Å) and were included in the refinement in the riding-model approximation,

with *U*<sub>iso</sub>(H) set to 1.2*U*<sub>eq</sub>(C). The nitrogen-bound H atom was located from difference-Fourier maps and refined with N–H = 0.88 ± 0.01 Å, and with *U*<sub>iso</sub>(H) set to 1.2*U*<sub>eq</sub>(N).

## Funding information

Crystallographic research at Sunway University is supported by Sunway University Sdn Bhd (grant No. STR-RCTR-RCCM-001–2019).

## References

- Arman, H. D., Poplalkhin, P. & Tiekink, E. R. T. (2018). *Z. Kristallogr. New Cryst. Struct.* **233**, 159–161.
- Brandenburg, K. (2006). *DIAMOND*. Crystal Impact GbR, Bonn, Germany.
- Dolomanov, O. V., Bourhis, L. J., Gildea, R. J., Howard, J. A. K. & Puschmann, H. (2009). *J. Appl. Cryst.* **42**, 339–341.
- Farrugia, L. J. (2012). *J. Appl. Cryst.* **45**, 849–854.
- Gans, J. & Shalloway, D. (2001). *J. Mol. Graph. Model.* **19**, 557–559.
- Goroff, N. S., Curtis, S. M., Webb, J. A., Fowler, F. W. & Lauher, J. W. (2005). *Org. Lett.* **7**, 1891–1893.
- Jotani, M. M., Zukerman-Schpector, J., Sousa Madureira, L., Poplalkhin, P., Arman, H. D., Miller, T. & Tiekink, E. R. T. (2016). *Z. Kristallogr.* **231**, 415–425.
- Lee, G.-H. (2010). *Acta Cryst.* **C66**, o241–o244.
- Lee, G.-H. & Wang, H.-T. (2007). *Acta Cryst.* **C63**, m216–m219.
- Macrae, C. F., Edgington, P. R., McCabe, P., Pidcock, E., Shields, G. P., Taylor, R., Towler, M. & van de Streek, J. (2006). *J. Appl. Cryst.* **39**, 453–457.
- Nguyen, T. L., Fowler, F. W. & Lauher, J. W. (2001). *J. Am. Chem. Soc.* **123**, 11057–11064.
- Nguyen, T. L., Scott, A., Dinkelmeyer, B., Fowler, F. W. & Lauher, J. W. (1998). *New J. Chem.* **22**, 129–135.
- Rigaku OD (2015). *CrysAlis PRO*. Rigaku Oxford Diffraction, Yarnton, England.
- Sheldrick, G. M. (2015a). *Acta Cryst.* **A71**, 3–8.
- Sheldrick, G. M. (2015b). *Acta Cryst.* **C71**, 3–8.
- Spackman, M. A. & Jayatilaka, D. (2009). *CrystEngComm*, **11**, 19–32.
- Syed, S., Jotani, M. M., Halim, S. N. A. & Tiekink, E. R. T. (2016). *Acta Cryst.* **E72**, 391–398.
- Tan, S. L., Jotani, M. M. & Tiekink, E. R. T. (2019). *Acta Cryst.* **E75**, 308–318.
- Tan, Y. S., Chun, H. Z., Jotani, M. M. & Tiekink, E. R. T. (2019). *Z. Kristallogr. Cryst. Mater.* **234**, 165–175.
- Tiekink, E. R. T. (2017). *Multi-Component Crystals: Synthesis, Concepts, Function*, edited by E. R. T. Tiekink & J. Schpector-Zukerman, pp. 289–319. De Gruyter: Singapore.
- Turner, M. J., Mckinnon, J. J., Wolff, S. K., Grimwood, D. J., Spackman, P. R., Jayatilaka, D. & Spackman, M. A. (2017). *Crystal Explorer 17*. The University of Western Australia.
- Westrip, S. P. (2010). *J. Appl. Cryst.* **43**, 920–925.
- Zukerman-Schpector, J., Sousa Madureira, L., Poplalkhin, P., Arman, H. D., Miller, T. & Tiekink, E. R. T. (2015). *Z. Kristallogr. Cryst. Mater.* **230**, 531–541.

## supporting information

*Acta Cryst.* (2019). E75, 1133-1139 [https://doi.org/10.1107/S2056989019009551]

## *N,N'*-Bis(pyridin-4-ylmethyl)oxalamide benzene monosolvate: crystal structure, Hirshfeld surface analysis and computational study

Sang Loon Tan, Nathan R. Halcovitch and Edward R. T. Tiekink

### Computing details

Data collection: *CrysAlis PRO* (Rigaku OD, 2015); cell refinement: *CrysAlis PRO* (Rigaku OD, 2015); data reduction: *CrysAlis PRO* (Rigaku OD, 2015); program(s) used to solve structure: SHELXT (Sheldrick, 2015a); program(s) used to refine structure: SHELXL2018 (Sheldrick, 2015b); molecular graphics: *ORTEP-3 for Windows* (Farrugia, 2012), *OLEX2* (Dolomanov *et al.*, 2009), *Mercury* (Macrae *et al.*, 2006), *DIAMOND* (Brandenburg, 2006) and *QMol* (Gans & Shalloway, 2001); software used to prepare material for publication: *publCIF* (Westrip, 2010).

### *N,N'*-Bis(pyridin-4-ylmethyl)oxalamide benzene monosolvate

#### Crystal data

$C_{14}H_{14}N_4O_2 \cdot C_6H_6$

$M_r = 348.40$

Monoclinic,  $P2_1/c$

$a = 5.80832$  (8) Å

$b = 12.6437$  (2) Å

$c = 12.1803$  (2) Å

$\beta = 99.942$  (1)°

$V = 881.07$  (2) Å<sup>3</sup>

$Z = 2$

$F(000) = 368$

$D_x = 1.313$  Mg m<sup>-3</sup>

Cu  $K\alpha$  radiation,  $\lambda = 1.54184$  Å

Cell parameters from 5470 reflections

$\theta = 3.7\text{--}76.1^\circ$

$\mu = 0.71$  mm<sup>-1</sup>

$T = 100$  K

Block, colourless

$0.27 \times 0.22 \times 0.16$  mm

#### Data collection

Rigaku Oxford Diffraction SuperNova, Dual,

Cu at zero, AtlasS2

diffractometer

Radiation source: micro-focus sealed X-ray

tube, SuperNova (Cu) X-ray Source

Mirror monochromator

Detector resolution: 5.2303 pixels mm<sup>-1</sup>

$\omega$  scans

Absorption correction: multi-scan

(*CrysAlis PRO*; Rigaku OD, 2015)

$T_{\min} = 0.917$ ,  $T_{\max} = 1.000$

7547 measured reflections

1838 independent reflections

1741 reflections with  $I > 2\sigma(I)$

$R_{\text{int}} = 0.018$

$\theta_{\max} = 76.3^\circ$ ,  $\theta_{\min} = 5.1^\circ$

$h = -7 \rightarrow 6$

$k = -15 \rightarrow 15$

$l = -14 \rightarrow 15$

#### Refinement

Refinement on  $F^2$

Least-squares matrix: full

$R[F^2 > 2\sigma(F^2)] = 0.034$

$wR(F^2) = 0.092$

$S = 1.03$

1838 reflections

121 parameters

1 restraint

Primary atom site location: structure-invariant

direct methods

Secondary atom site location: difference Fourier

map

Hydrogen site location: mixed

H atoms treated by a mixture of independent  
and constrained refinement  
 $w = 1/[\sigma^2(F_o^2) + (0.052P)^2 + 0.2834P]$   
where  $P = (F_o^2 + 2F_c^2)/3$

$(\Delta/\sigma)_{\max} < 0.001$   
 $\Delta\rho_{\max} = 0.26 \text{ e } \text{\AA}^{-3}$   
 $\Delta\rho_{\min} = -0.22 \text{ e } \text{\AA}^{-3}$

### Special details

**Geometry.** All esds (except the esd in the dihedral angle between two l.s. planes) are estimated using the full covariance matrix. The cell esds are taken into account individually in the estimation of esds in distances, angles and torsion angles; correlations between esds in cell parameters are only used when they are defined by crystal symmetry. An approximate (isotropic) treatment of cell esds is used for estimating esds involving l.s. planes.

### Fractional atomic coordinates and isotropic or equivalent isotropic displacement parameters ( $\text{\AA}^2$ )

	<i>x</i>	<i>y</i>	<i>z</i>	$U_{\text{iso}}^*/U_{\text{eq}}$
O10	0.38046 (13)	0.37705 (6)	0.02822 (6)	0.02248 (19)
N1	1.08230 (15)	0.16191 (7)	0.27845 (7)	0.0201 (2)
N8	0.60308 (14)	0.49128 (6)	0.14611 (7)	0.01478 (19)
H8N	0.681 (2)	0.5518 (8)	0.1539 (10)	0.018*
C2	0.90416 (19)	0.16751 (8)	0.33490 (9)	0.0212 (2)
H2	0.886428	0.111791	0.385095	0.025*
C3	0.74433 (18)	0.24969 (8)	0.32443 (8)	0.0182 (2)
H3	0.619613	0.249378	0.365660	0.022*
C4	0.76959 (16)	0.33301 (7)	0.25225 (8)	0.0146 (2)
C5	0.95261 (17)	0.32732 (8)	0.19256 (8)	0.0166 (2)
H5	0.974925	0.381952	0.141884	0.020*
C6	1.10251 (17)	0.24105 (8)	0.20768 (8)	0.0179 (2)
H6	1.225774	0.237994	0.165662	0.022*
C7	0.60511 (16)	0.42643 (8)	0.24442 (8)	0.0154 (2)
H7A	0.444777	0.400031	0.244779	0.018*
H7B	0.649954	0.471177	0.311395	0.018*
C9	0.49063 (16)	0.46013 (7)	0.04685 (8)	0.0152 (2)
C11	0.4304 (2)	0.59937 (9)	0.45845 (8)	0.0238 (2)
H11	0.382675	0.667329	0.429930	0.029*
C12	0.27389 (19)	0.51554 (9)	0.44356 (9)	0.0244 (2)
H12	0.119021	0.526258	0.404969	0.029*
C13	0.3429 (2)	0.41613 (9)	0.48487 (9)	0.0240 (2)
H13	0.235695	0.358784	0.474473	0.029*

### Atomic displacement parameters ( $\text{\AA}^2$ )

	$U^{11}$	$U^{22}$	$U^{33}$	$U^{12}$	$U^{13}$	$U^{23}$
O10	0.0285 (4)	0.0190 (4)	0.0182 (4)	-0.0090 (3)	-0.0007 (3)	0.0018 (3)
N1	0.0205 (4)	0.0181 (4)	0.0208 (4)	0.0028 (3)	0.0012 (3)	0.0003 (3)
N8	0.0163 (4)	0.0123 (4)	0.0153 (4)	-0.0007 (3)	0.0016 (3)	0.0012 (3)
C2	0.0249 (5)	0.0181 (5)	0.0202 (5)	0.0010 (4)	0.0027 (4)	0.0047 (4)
C3	0.0195 (5)	0.0190 (5)	0.0166 (5)	-0.0002 (4)	0.0041 (4)	0.0013 (4)
C4	0.0152 (4)	0.0151 (5)	0.0126 (4)	-0.0010 (3)	-0.0007 (3)	-0.0016 (3)
C5	0.0174 (5)	0.0164 (5)	0.0156 (5)	-0.0016 (4)	0.0019 (4)	0.0005 (3)
C6	0.0168 (5)	0.0191 (5)	0.0177 (5)	-0.0001 (4)	0.0024 (4)	-0.0019 (4)

C7	0.0166 (4)	0.0161 (5)	0.0136 (4)	0.0008 (3)	0.0031 (3)	0.0003 (3)
C9	0.0146 (4)	0.0148 (5)	0.0161 (5)	0.0011 (3)	0.0025 (4)	0.0012 (4)
C11	0.0337 (6)	0.0228 (5)	0.0169 (5)	0.0095 (4)	0.0098 (4)	0.0043 (4)
C12	0.0201 (5)	0.0372 (6)	0.0164 (5)	0.0070 (4)	0.0050 (4)	0.0025 (4)
C13	0.0289 (6)	0.0275 (6)	0.0175 (5)	-0.0041 (4)	0.0091 (4)	-0.0014 (4)

*Geometric parameters (Å, °)*

O10—C9	1.2305 (12)	C5—C6	1.3879 (14)
N1—C2	1.3394 (14)	C5—H5	0.9500
N1—C6	1.3391 (13)	C6—H6	0.9500
N8—C9	1.3307 (13)	C7—H7A	0.9900
N8—C7	1.4496 (12)	C7—H7B	0.9900
N8—H8N	0.886 (8)	C9—C9 <sup>i</sup>	1.5406 (18)
C2—C3	1.3845 (14)	C11—C12	1.3876 (17)
C2—H2	0.9500	C11—C13 <sup>ii</sup>	1.3911 (16)
C3—C4	1.3961 (14)	C11—H11	0.9500
C3—H3	0.9500	C12—C13	1.3871 (16)
C4—C5	1.3895 (14)	C12—H12	0.9500
C4—C7	1.5118 (13)	C13—H13	0.9500
C2—N1—C6	116.89 (9)	N8—C7—C4	114.14 (8)
C9—N8—C7	121.05 (8)	N8—C7—H7A	108.7
C9—N8—H8N	121.0 (8)	C4—C7—H7A	108.7
C7—N8—H8N	118.0 (8)	N8—C7—H7B	108.7
N1—C2—C3	123.89 (9)	C4—C7—H7B	108.7
N1—C2—H2	118.1	H7A—C7—H7B	107.6
C3—C2—H2	118.1	O10—C9—N8	125.33 (9)
C2—C3—C4	118.86 (9)	O10—C9—C9 <sup>i</sup>	121.53 (11)
C2—C3—H3	120.6	N8—C9—C9 <sup>i</sup>	113.14 (10)
C4—C3—H3	120.6	C12—C11—C13 <sup>ii</sup>	119.98 (10)
C5—C4—C3	117.62 (9)	C12—C11—H11	120.0
C5—C4—C7	122.66 (9)	C13 <sup>ii</sup> —C11—H11	120.0
C3—C4—C7	119.70 (9)	C13—C12—C11	120.20 (10)
C4—C5—C6	119.36 (9)	C13—C12—H12	119.9
C4—C5—H5	120.3	C11—C12—H12	119.9
C6—C5—H5	120.3	C12—C13—C11 <sup>ii</sup>	119.82 (11)
N1—C6—C5	123.37 (9)	C12—C13—H13	120.1
N1—C6—H6	118.3	C11 <sup>ii</sup> —C13—H13	120.1
C5—C6—H6	118.3		
C6—N1—C2—C3	-0.44 (15)	C9—N8—C7—C4	76.76 (11)
N1—C2—C3—C4	-0.91 (16)	C5—C4—C7—N8	19.14 (13)
C2—C3—C4—C5	1.46 (14)	C3—C4—C7—N8	-162.91 (8)
C2—C3—C4—C7	-176.60 (9)	C7—N8—C9—O10	0.23 (15)
C3—C4—C5—C6	-0.74 (14)	C7—N8—C9—C9 <sup>i</sup>	-179.96 (9)
C7—C4—C5—C6	177.26 (8)	C13 <sup>ii</sup> —C11—C12—C13	-0.13 (17)

C2—N1—C6—C5	1.23 (15)	C11—C12—C13—C11 <sup>ii</sup>	0.13 (17)
C4—C5—C6—N1	-0.64 (15)		

Symmetry codes: (i)  $-x+1, -y+1, -z$ ; (ii)  $-x+1, -y+1, -z+1$ .

*Hydrogen-bond geometry (Å, °)*

*Cg*1 is the centroid of the centrosymmetric (C11–C13, C11<sup>i</sup>–C13<sup>i</sup>) ring. *Cg*2 is the ring centroid of the (N1, C2–C5) ring.

<i>D</i> —H $\cdots$ <i>A</i>	<i>D</i> —H	H $\cdots$ <i>A</i>	<i>D</i> $\cdots$ <i>A</i>	<i>D</i> —H $\cdots$ <i>A</i>
N8—H8N $\cdots$ O10 <sup>i</sup>	0.89 (1)	2.36 (1)	2.7129 (11)	104 (1)
N8—H8N $\cdots$ N1 <sup>iii</sup>	0.89 (1)	2.03 (1)	2.8737 (12)	159 (1)
C7—H7B $\cdots$ <i>Cg</i> 1	0.99	2.62	3.4037 (11)	136
C11—H11 $\cdots$ <i>Cg</i> 2 <sup>iv</sup>	0.95	2.90	3.6361 (11)	136

Symmetry codes: (i)  $-x+1, -y+1, -z$ ; (iii)  $-x+2, y+1/2, -z+1/2$ ; (iv)  $-x+1, y+1/2, -z+1/2$ .